Crystal structures and magnetic properties of $Fe_{1.93-x}Co_xP_{1-y}Si_y$ compounds

Bao, L. L.; Yibole, H.; Xu, J. Y.; Ou, Z. Q.; Haschuluu, O.; Tegus, O.; van Dijk, N. H.; Brück, E.; Guillou, F.

DOI
10.1016/j.jallcom.2022.163770

Publication date
2022

Document Version
Final published version

Published in
Journal of Alloys and Compounds

Journal of Alloys and Compounds 903 (2022) 163770

Contents lists available at ScienceDirect

Journal of Alloys and Compounds

journal homepage: www.elsevier.com/locate/jalcom

Crystal structures and magnetic properties of $Fe_{1.93-x}Co_xP_{1-y}Si_y$ compounds

L.L. Bao[a], H. Yibole[a,*], J.Y. Xu[a], Z.Q. Ou[a], O. Haschuluu[a], O. Tegus[a], N.H. van Dijk[b], E. Brück[b], F. Guillou[a]

[a] College of Physics and Electronic Information, Inner Mongolia Key Laboratory for Physics and Chemistry of Functional Materials, Inner Mongolia Normal University, Hohhot 010022, China
[b] FAME Group, Department of Radiation Science & Technology, Delft University of Technology, Mekelweg 15, 2629JB Delft, The Netherlands

ARTICLE INFO

Article history:
Received 3 November 2021
Received in revised form 20 December 2021
Accepted 11 January 2022
Available online 13 January 2022

Keywords:
Crystal structure
Phase diagrams
Magnetic measurements
Permanent magnets

ABSTRACT

In view of the interest that $(Fe,Co)_2(P,Si)$ compounds have as potential permanent magnets, their structural and magnetic phase diagrams are explored focusing on establishing the range where the hexagonal Fe_2P-type structure is observed. In $Fe_{1.93-x}Co_xP_{1-y}Si_y$, the highest Si content prior entering a mixed phase domain is $y \approx 0.5$. At high Si content but low Co for Fe substitutions, a structural distortion leading to a body-centered orthorhombic structure occurs. At high Co contents, when the Fe_2P unit cell reaches a critical volume of about 102.4 Å^3, the samples crystallize in a Co_2P-type orthorhombic structure. Within the Fe_2P-type structural range, the evolution of the unit-cell volume appears to follow the Vegard's law, but this hides strongly anisotropic changes. Simultaneous Co for Fe and Si for P substitutions increase the range where the hexagonal structure is observed in comparison to ternary $Fe_2(P,Si)$ and $(Fe,Co)_2P$. The samples are ferromagnetic, but with Curie temperatures showing an unusual evolution, uncorrelated to the *c/a* ratio of the lattice parameters. At low Si content, T_C increases with Co for Fe substitutions. For $y = 0.2$, the evolution is not significant, while at high Si content T_C systematically decreases with the increase in Co. Large Si and Co substitutions lead to a swift weakening of the magnetocrystalline anisotropy until the easy axis anisotropy turns from the *c* axis toward the *a-b* plane. This study guides future investigations by restricting the range where desirable properties for permanent magnetic applications can be expected to $0.1 \lesssim x \lesssim 0.3$ and $0.1 \lesssim y \lesssim 0.3$.

1. Introduction

Potential permanent magnetic materials deriving from Fe_2P are experiencing a renewed theoretical and experimental interest. Since this materials family is based on iron, the most abundant magnetic element, it makes these materials appealing for applications. The permanent magnet market is nowadays dominated by two materials families. On the one hand, the low-cost and of non-critical supply ferrites ($BaFe_{12}O_{19}$, $SrFe_{12}O_{19}$ and related) are the most widely used magnets, yet they exhibit low performances. On the other hand, high-performance permanent magnets such as Nd-Fe-B materials can show very high $|BH|_{max}$ energy products, but require doping with heavy rare-earths, making them scarce and expensive. As a result, much efforts are currently targeted at developing rare-earth-free permanent magnets, in particular focusing on materials having the potential to present a higher performance than the ferrites and a lower cost than that of rare-earth magnets [1–4], as is the case for Fe_2P-type materials.

The binary Fe_2P parent crystallizes into a hexagonal structure ($P\bar{6}2m$) and presents a strong magnetocrystalline anisotropy with the easy magnetic axis corresponding to the crystallographic *c* axis. But its Curie temperature ($T_C = 214$ K) is too low for permanent magnet applications [5–8]. In order to increase T_C, substitutions can be made either on the metal site such as in $(Fe,Co)_2P$ and $(Fe,Ni)_2P$ or on the metalloid sites like in $Fe_2(P,As)$, $Fe_2(P,Ge)$, $Fe_2(P,Si)$ or $Fe_2(P,B)$ [9–13]. All these ternary substitutions can lead to an increase in Curie temperature, but also result in the appearance of competing crystal structures and a reduced magnetic anisotropy. Nevertheless, permanent magnets were successfully prepared. De Vos et al. achieved coercive field $\mu_0 H_C = 0.22$ T at room temperature in $Fe_{1.7}Co_{0.3}P$ particles prepared by lixiviating a Fe-Co-Cu-P melt [14]. Ultrafine $Fe_{1.7}Co_{0.3}P$ particles (28 nm) produced by a gas phase

* Corresponding author.
E-mail address: hyibole@imnu.edu.cn (H. Yibole).

https://doi.org/10.1016/j.jallcom.2022.163770
0925-8388/

reaction reached a coercitivity of $\mu_0 H_C$ = 0.39 T at room temperature [15]. Even smaller $Fe_{1.8}Co_{0.2}P$ particles (21.8 ± 3.6 nm) can be prepared by the solution-phase method, but this particle size leads to the appearance of a superparamagnetic behavior with a lower Curie temperature than the bulk and the appearance of a blocking temperature, which are both undesirable for permanent magnet applications [16]. So far, improvements of the permanent magnetic properties in the Fe_2P system have mostly been reached through control of the microstructure rather than compositional adjustments. Yet, very recent theoretical and experimental studies revealed that quaternary compositions can be more promising than $(Fe,Co)_2P$ ternary compounds [17–21]. A preliminary study on $Fe_{1.80}Co_{0.20}P_{1-y}Si_y$ and $Fe_{1.75}Co_{0.20}P_{1-y}Si_y$ powders oriented in magnetic field suggested the possibility to combine high Curie temperatures (up to 640 K) with uniaxial magnetocrystalline anisotropy [18]. Subsequently, a study employing single crystals confirmed that a large magnetocrystalline anisotropy ($K_1 \approx 0.9$ MJm^{-3}) is reachable at room temperature and in addition demonstrated that permanent magnetic properties could be achieved in $(Fe,Co)_2(P,Si)$ quaternary alloys via particle size reduction with a room temperature coercitivity of $\mu_0 H_C \approx 0.2$ T and an energy product $|BH|_{max} \approx 5$ kJ m^{-3} [20]. Another single-crystal study on quaternary $(Fe,Co)_2(P,Si)$ demonstrated even larger room-temperature magnetic anisotropy of $K_1 \approx 1.09$ MJm^{-3} in $Fe_{1.82}Co_{0.18}P_{0.78}Si_{0.22}$ and suggested that much larger energy products should be reachable with a theoretical $|BH|_{max}$ up to 204 kJ m^{-3} [21].

Further developments are however impeded by the absence of a structural phase diagram for quaternary $(Fe,Co)_2(P,Si)$ compounds. In $Fe_{2-x}Co_xP$ ternary compounds, Co substitutions trigger a crystal structure change from the hexagonal Fe_2P-type to the orthorhombic Co_2P-type (space group *Pnma*) around $x \approx 0.32$ [9]. In $Fe_2P_{1-y}Si_y$ ternary compounds, Si substitutions lead to a spectacular increase in Curie temperature, but a competing body-centered orthorhombic (BCO, space group *Imm*2) phase appears at room temperature around $y \approx 0.2$ [12]. A first study on $Fe_{1.80}Co_{0.20}P_{1-y}Si_y$ indicates that simultaneous Co and Si substitutions could expand the stability range of the Fe_2P-type structure beyond what is achievable in ternary compounds [18]. Yet, it is not clear up to which substitution levels the hexagonal Fe_2P-type structure can be preserved. Unfortunately, the known phase diagrams of closely related quaternaries, such as magnetocaloric $Mn_{2-x}Fe_xP_{1-y}Si_y$ are of little help, as their end compositions involve different crystal structures. The primary goal of the present study is therefore to explore the structural phase diagram of $Fe_{2-x}Co_xP_{1-y}Si_y$ compounds, focusing in particular on the stability range of the hexagonal Fe_2P-type structure and on the relationships between the different structures at play. Magnetic measurements were carried out in order to establish structure-properties relationship for hexagonal $Fe_{2-x}Co_xP_{1-y}Si_y$ compounds with a special emphasis on magnetic parameters relevant for permanent magnet applications, i.e. the Curie temperature and the magnetocrystalline anisotropy. In view of the difficulties met in growing $(Fe,Co)_2(P,Si)$ single crystals of specifically targeted compositions and the apparent impossibility to grow crystals with a high Si content (y is typically lower than $y < 0.35$ in single crystals) [20], polycrystalline materials prepared by mechanical alloying followed by a solid-state reaction are presently investigated.

2. Experimental details

Several series of $Fe_{1.93-x}Co_xP_{1-y}Si_y$ quaternary compounds were prepared with Si contents fixed at y = 0.1, 0.2, 0.3, 0.4 and 0.5 and Co contents varied from x = 0–1.2. A total number of thirty-eight samples was selected to cover the investigated composition range. Elemental starting materials were ball-milled using stainless steel jars in a planetary mill at a speed of 350 rpm for 10 h. The sample-to-ball mass ratio was 1:5. The resulting powders were pressed in a mold of 10 mm inner diameter and sealed in quartz ampules backfilled with 200 mbar Ar. The heat treatment consisted of a single annealing at 1100 °C for 22 h followed by quenching in water. Powder x-ray diffraction and magnetic orientation were obtained on hand-crushed samples and sieving the powders to less than 36 µm. Epoxy bonded powders were prepared at a high dilution mass ratio of 1:1 (correct dispersion and orientation of the particles is more crucial in the present study than maximizing the density), then shaped into plates of approximately 15 × 30 × 2 mm^3, and oriented in a $\mu_0 H$ = 1.1 T magnetic field with the plate surface normal to the orientation of the magnetic field.

Powder X-ray diffraction (XRD) experiments were performed on an Empyrean PANalytical diffractometer using Cu-K_α radiation over a 20–90° 2θ angular range. The Rietveld method as implemented in the FullProf software is used for structural refinements [22] and the VESTA software is used for crystal structure visualization [23].

Magnetic measurements were conducted in a Quantum Design Versalab system equipped with a vibrating sample magnetometer option. For high-temperature magnetic measurements (T > 400 K), a Lakeshore 7407 vibrating sample magnetometer equipped with a high temperature furnace was used.

3. Results and discussion

3.1. Stability range of the Fe_2P-type crystal structure

To assess the stability of the Fe_2P hexagonal structure in $(Fe,Co)_2(P,Si)$ compounds, the phase diagram was explored by focusing on $Fe_{1.93-x}Co_xP_{1-y}Si_y$ quaternary compounds with Si in the range $0 \le y \le 0.5$ and $0 \le x < 1.2$ for Co. From former studies on magnetocaloric $(Mn,Fe)_2(P,Si)$ and $Fe_{1.80}Co_{0.20}(P,Si)$ [18,24], the under-stoichiometry in metal:metalloid ratio appears as a pragmatic solution to reduce the secondary phase contamination. In particular, it limits the formation of cubic Fe_3Si-type phase which is favored by the increase in Si content. Fig. 1 illustrates the competition between the different crystal structures in $Fe_{1.93-x}Co_xP_{1-y}Si_y$ quaternary compounds by taking the example of a series of samples at fixed Si content y = 0.4. The powder XRD pattern of the ternary $Fe_{1.93}P_{0.60}Si_{0.40}$ (x = 0, not shown) compound was refined in the formerly reported BCO structure [12]. A limited Co substitution (x = 0.1) preserves the BCO structure, yet a further Co increase to x = 0.2 triggers a transformation toward the hexagonal Fe_2P-type structure (see Fig. 1). The hexagonal structure is stable until relatively large Co content (x = 1.0), above which the structure turns into an orthorhombic Co_2P-type structure. We note that all diffraction patterns present additional peaks characteristic of 3:1 secondary phase. The samples shown in Fig. 1 present an additional peak near 45°

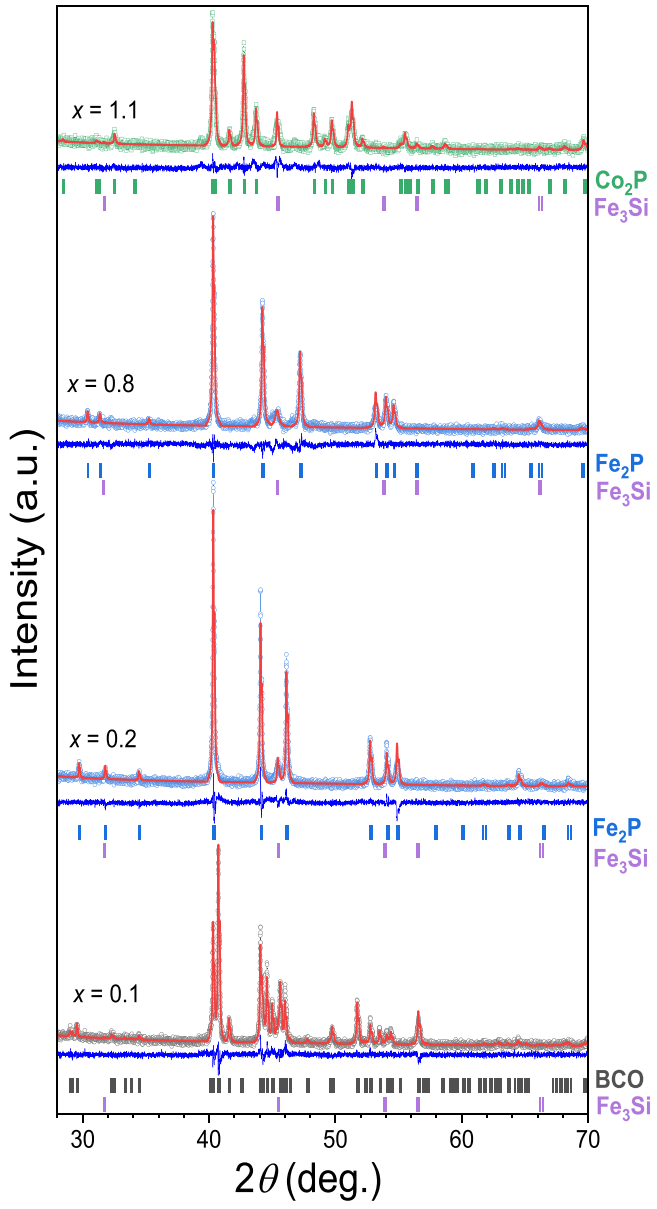

Fig. 1. Powder X-ray diffraction patterns for $Fe_{1.93-x}Co_xP_{0.6}Si_{0.4}$ compounds, with selected representative compositions from $x = 0.1$ (bottom) to $x = 1.1$ (top). The symbols mark the observed intensity, the overlaid line the intensity calculated by refinement, the line below is the difference between observed and calculated intensities, and the ticks mark the position of the reflections from the different structures.

characteristic of a Fe_3Si-type cubic secondary phase, whose weight fraction remains however limited, of the order of 3–4 wt%. Samples with low Si content ($y \leq 0.1$) also show the presence of a 3:1 secondary phase, but having a tetragonal crystal structure similar to that of Fe_3P. In a similar manner as a former study on $Fe_{1.8}Co_{0.2}P_{1-y}Si_y$ compounds [18], the nature of the secondary phase evolves with the nominal composition.

Scanning electron microscopy (SEM) coupled with energy dispersive X-ray spectroscopy (EDX) was carried out on several representative samples. Fig. 2 and Table 1 illustrate the results for selected $Fe_{1.93-x}Co_xP_{0.6}Si_{0.4}$ compounds. In general, SEM imaging reveals a significant porosity, and backscattered electron imaging or EDX elemental mapping shows the presence of a secondary phase. The local composition of the secondary phase is close to Fe_3Si, confirming the interpretation of powder XRD data. We note that the formation of a secondary phase with a metal:metalloid ratio close to 3:1 leads to a further off-stoichiometry of the main phase below 1.93:1. This suggests that the formation of 3:1 secondary phase results from its inherent stability rather than being promoted by phosphorous losses during the synthesis. In addition, the secondary 3:1 phase is a Si-rich phase, which leads to a reduced Si content in the matrix. These observations are in line with that previously made on $(Fe,Co)_2P_{0.8}Si_{0.2}$ compounds with a nominal 2:1 metal:metalloid ratio and with $(Mn,Fe)_{1.95}(P,Si)$ studies [18,24].

Fig. 3 shows the structural phase diagram of $Fe_{1.93-x}Co_xP_{1-y}Si_y$ compounds built from powder XRD data at room temperature. The highest Si content considered was $y = 0.5$. For $y > 0.5$, samples were no longer (nearly) single-phase, as they contain large amounts of various phases: cubic Fe_3Si-type, hexagonal Fe_5Si_3-type and Fe_2P-type phases. $Fe_{1.93-x}Co_xP_{1-y}Si_y$ samples with $y = 0.5$ already present an increased Fe_3Si-type secondary phase content in comparison to the $y = 0.4$ samples displayed in Fig. 1 (from refinement of powder XRD data, the secondary phase fraction is in the range 6–9 wt%, for $y = 0.5$ samples). For ternary $Fe_{1.93}P_{1-y}Si_y$ compounds or quaternary $Fe_{1.93-x}Co_xP_{1-y}Si_y$ with a low Co content, the increase in Si content favors the formation of the BCO structure, which is somewhat similar to the structural phase diagram of the closely related $Fe_{1.95-x}Ni_xP_{1-y}Si_y$ compounds [19]. But in contrast to the latter, at fixed Si content, high Co substitutions eventually lead to the formation of a Co_2P-type orthorhombic structure. Despite the competing structures, the hexagonal Fe_2P-type clearly benefits from simultaneous metal and metalloid substitutions as its stability range is increased compared to the corresponding ternary compounds. Limited to $x \leq 0.3$ in $Fe_{2-x}Co_xP$, the Co content acceptable in the Fe_2P-type structure now ranges up to $x = 1.0$ in $Fe_{1.93-x}Co_xP_{0.6}Si_{0.4}$ quaternary compounds, offering –in principle– more freedom to tune their magnetic properties.

3.2. Structural relationships amongst $Fe_{1.93-x}Co_xP_{1-y}Si_y$ compounds

In order to address the evolution of the crystal structure as a function of the composition in more detail, we will first present the relationship between the three structures at play. Usually, the structure of *MM'X* compounds, where *M* and *M'* are transition metals and *X* a metalloid or non-metal, is described by analyzing the shortest metal-nonmetal distances and consider the coordination polyhedral surrounding the metallic element. Following this approach, the Fe_2P-type hexagonal structure ($P\bar{6}2m$) is described by two inequivalent metal sites 3*f* (x_f,0,0) and 3*g* (x_g,0,1/2) as well as two inequivalent metalloid sites 2*c* (1/3,2/3,0) and 1*b* (0,0,1/2). This corresponds to two distinct local geometries for the metal sites: the 3*f* site sits in a tetrahedral environment created by four metalloid atoms (two 2*c* and two 1*b* sites) and the 3*g* site is positioned in a square-based pyramidal environment surrounded by 5 metalloids.

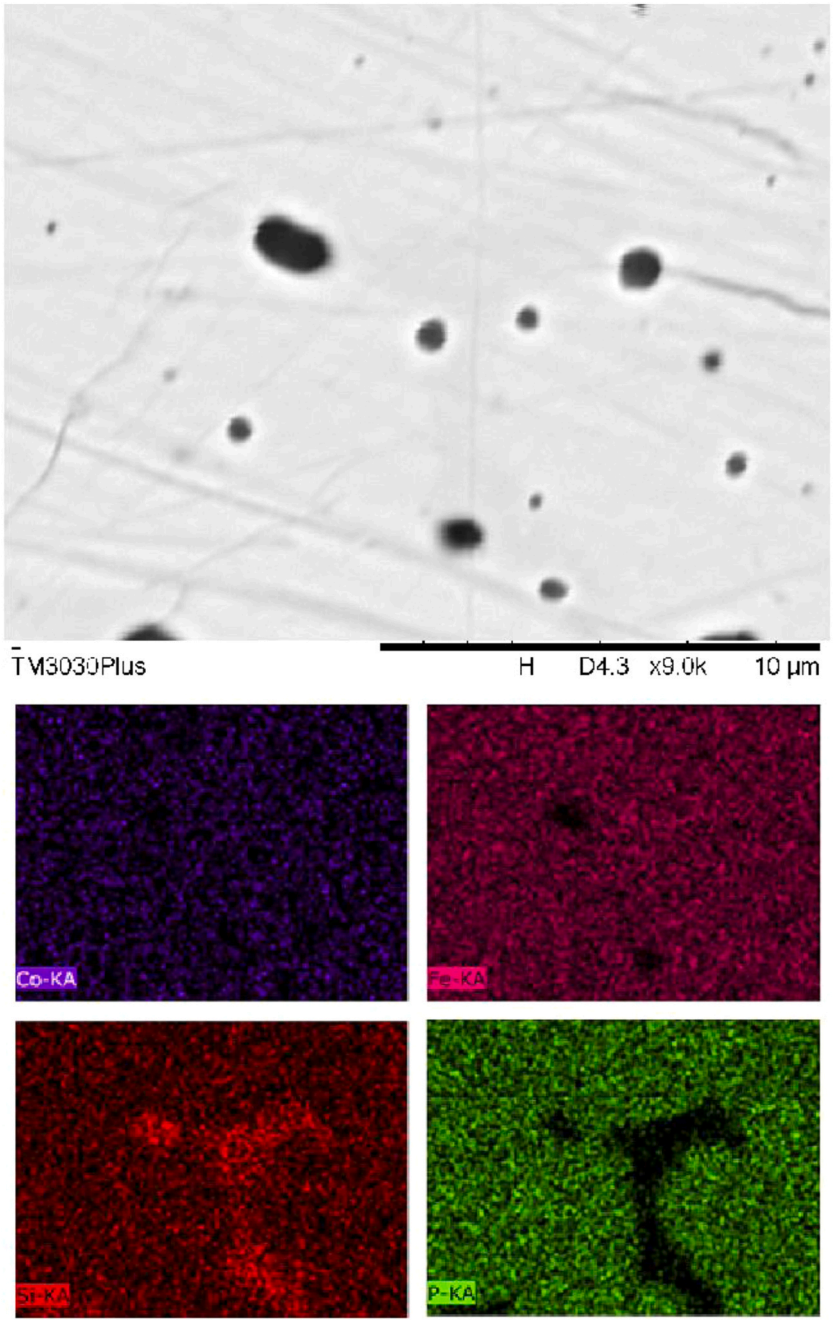

Fig. 2. SEM picture and EDX mapping of a polycrystalline $Fe_{1.83}Co_{0.10}P_{0.60}Si_{0.40}$ sample. Spot selected to highlight the presence of a secondary phase.

Table 1
EDX analyses for representative $Fe_{1.93-x}Co_xP_{0.6}Si_{0.4}$ samples crystallizing in the BCO, Fe_2P, and Co_2P-type structures (from top to bottom, respectively).

Nominal composition	Fe at%	Co at%	P at%	Si at%	Effective composition
$Fe_{1.83}Co_{0.10}P_{0.60}Si_{0.40}$ matrix	62.8(2.0)	2.8(0.1)	21.8(0.5)	12.6(0.3)	$Fe_{1.84}Co_{0.08}P_{0.64}Si_{0.37}$
inclusion	71.0(1.9)	1.5(0.1)	1.0(0.1)	26.5(0.5)	$Fe_{2.84}Co_{0.06}P_{0.04}Si_{1.06}$
$Fe_{1.53}Co_{0.40}P_{0.60}Si_{0.40}$	52.3(1.6)	11.3(0.5)	21.4(0.6)	15.0(0.5)	$Fe_{1.53}Co_{0.33}P_{0.63}Si_{0.44}$
$Fe_{0.83}Co_{1.10}P_{0.60}Si_{0.40}$	31.3(1.1)	35.7(1.3)	21.0(0.6)	12.0(0.3)	$Fe_{0.92}Co_{1.05}P_{0.62}Si_{0.35}$

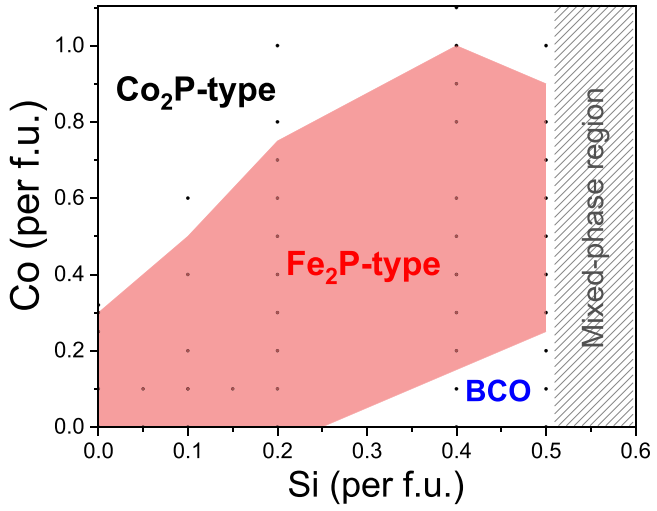

Fig. 3. Structural phase diagram for $Fe_{1.93-x}Co_xP_{1-y}Si_y$ compounds built from the analysis of room temperature powder X-ray diffraction data.

The metalloid polyhedrons surrounding the metal sites are illustrated in Fig. 4. Similar metallic environments can be distinguished both in the BCO and the Co_2P-type structures. The link between the sites (Wyckoff positions) for the different structures is provided in Table 2. The primary difference between the three structures is in the stacking of tetrahedral and pyramidal metallic sites. In the hexagonal Fe_2P structure, tetrahedrons and square based-pyramids perfectly pile up along the (001) direction forming canals of triangular cross-section. Compared to Fe_2P, the BCO structure is born from a small displacement of the metallic atoms in the tetrahedrons along the (100) direction, which distorts the canal of triangular cross-section and leads to the appearance of a small zigzag along the metalloid chains. On the other hand, the Co_2P structure preserves the alignment of the triangular canals, but corresponds to a stacking of tetrahedral and pyramidal sites that is very different from the one in the Fe_2P structure. Transforming the Fe_2P structure to the Co_2P structure requires major displacements of the metalloid atoms, which may explain why Fe_2P-type to Co_2P-type structural transitions are observed only at high temperature in $(Fe,Co)_2P$ ternary compounds [14]. On the other hand, transforming from BCO to Fe_2P corresponds to a relatively minor distortion, so that the BCO-Fe_2P structural transition can be observed even below room temperature in $Fe_2(P,Si)$ ternary compounds [12].

Fig. 5 shows the hexagonal lattice parameters a and c, the lattice parameter ratio c/a and the unit-cell volume V of $Fe_{1.93-x}Co_xP_{1-y}Si_y$ compounds. Within the stability range of the Fe_2P structure, Si for P substitutions increase the cell volume, while Co for Fe decrease it, both evolutions being in line with their respective elemental atomic radii. Moreover, Co for Fe substitutions lead to a nearly linear evolution of the unit-cell volume within the Fe_2P-type stability range. Yet, this apparent agreement of the cell volume with the Vegard's law masks a strong anisotropic distortion of the unit cell, with the a axis decreasing and the c axis increasing with Co substitutions, both in a non-linear manner. These evolutions are somewhat at odds with the behavior of $(Fe,Co)_2P$ ternary compounds, where both the a and c axes were found to decrease [9]. If we however look at the structural evolution as a function of Si for P substitutions while Co content is fixed, we can notice a progressive unit-cell volume increase until y reaches the range 0.4–0.5, with $y = 0.5$ showing little to no evolution compared to $y = 0.4$. Compounds with $y = 0.5$ mark the boundary were a mixed phase region appears and are already anomalous, as the larger Fe_3Si-type secondary phase content compared to other samples leads to an understoichiometry in Si of the main phase. Using the equivalence $a_{ortho} = 2c_{hexa}$, $b_{ortho} = \sqrt{3}\,a_{hexa}$ and $c_{ortho} = a_{hexa}$, the BCO to Fe_2P phase boundary corresponds to a jump like increase in unit-cell volume with increasing Co content, as illustrated by the $y = 0.4$ series. This suggests that the distortion leading to the formation of the BCO structure originates from the impossibility to accommodate a significant amount of large Si atoms in the Fe_2P structure. At the other side of the Fe_2P stability range, the boundary between Fe_2P and Co_2P in the present $Fe_{1.93-x}Co_xP_{1-y}Si_y$ compounds seems to correspond to critical values of ratio $c/a \approx 0.59 \pm 0.002$ and cell volume $V \approx 102.40 \pm 0.02$ Å^3 that cannot be overcome. It is therefore likely that the large Co content that can preserve the hexagonal Fe_2P structure in $Fe_{1.93-x}Co_xP_{1-y}Si_y$ (up to $x = 1.0$), compared to the ternary $(Fe,Co)_2P$ (up to $x = 0.3$), originates from the ability of Si to compensate for the unit-cell volume contraction.

3.3. Magnetic properties of $Fe_{1.93-x}Co_xP_{1-y}Si_y$ compounds

Panel a) from Fig. 6 illustrates the temperature dependence of the magnetization for $Fe_{1.93-x}Co_xP_{0.9}Si_{0.1}$ compounds and panel b) summarizes the evolution of the Curie temperature. The magnetization curves present a two steps behavior with the first one corresponding to the Curie temperature of the main phase with the Fe_2P structure for $0.1 \le x \le 0.4$ or the Co_2P structure for $x = 0.6$ and the second step is the Curie temperature of the secondary phase with a 3:1 metal:metalloid ratio (recalling that the step amplitude is not directly representative for the phase content at low applied magnetic fields). The Curie temperatures of the secondary phase vary for different nominal compositions, mimicking the evolution of the nature of the 3:1 secondary phase. The Curie temperatures of the main phase were defined as the main minima of the dM/dT curves. For $y = 0.1$, the Curie temperature increases with the increase in Co content, up to $T_C \approx 480$ K for $x = 0.4$, then T_C slightly decreases when reaching the Co_2P structure for $x = 0.6$. This evolution of T_C with Co content in the $y = 0.1$ series is similar to that found in $Fe_{2-x}Co_xP$ ternary compounds showing an increase in T_C with Co substitutions until reaching the orthorhombic range [9]. However, at higher Si contents, the evolution of the Curie temperature is anomalous from

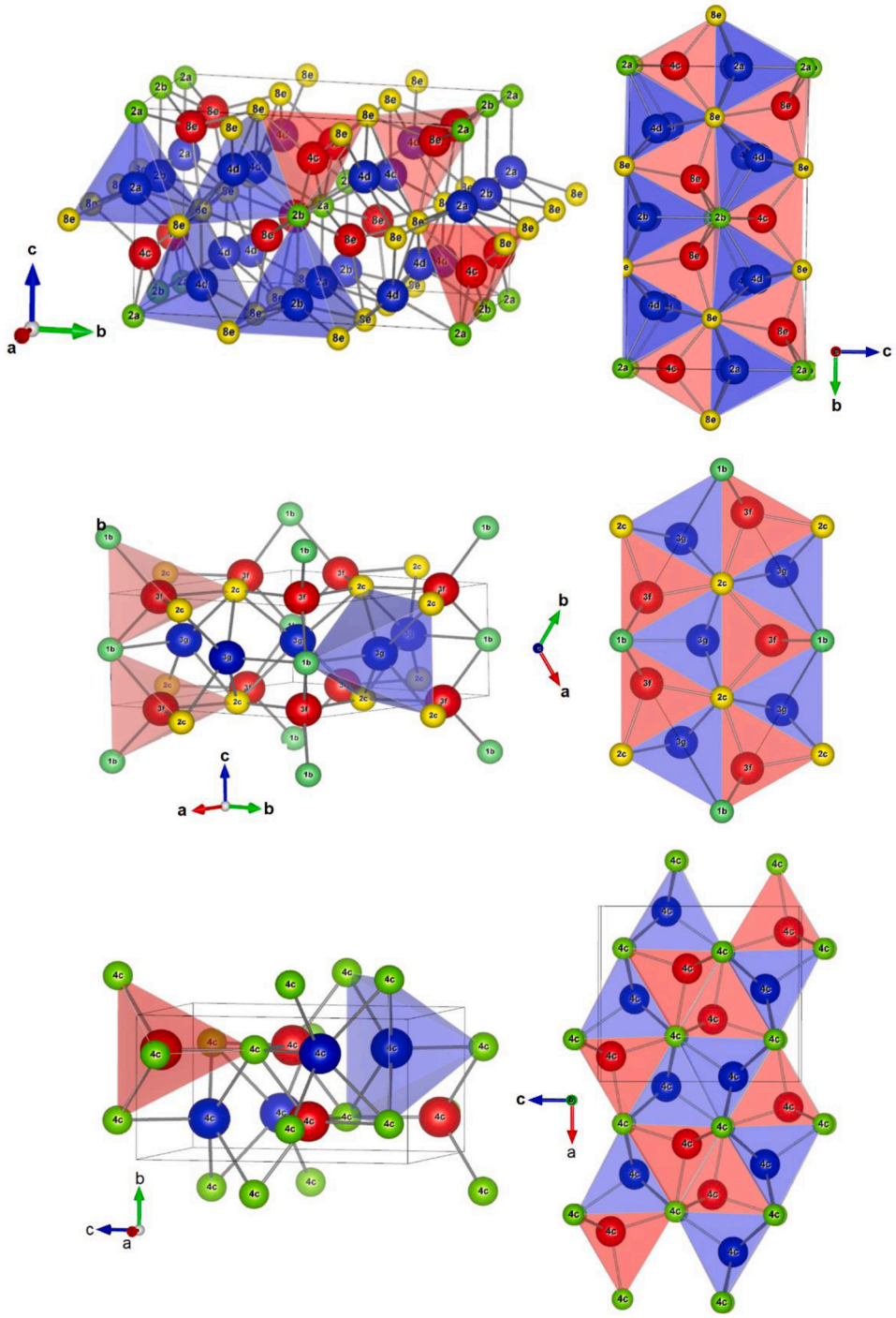

Fig. 4. Crystal structure representation for the BCO structure (top, $Fe_{1.83}Co_{0.1}P_{0.6}Si_{0.4}$), Fe_2P-type structure (middle, $Fe_{1.73}Co_{0.2}P_{0.6}Si_{0.4}$), and Co_2P-type structure (bottom, $Fe_{0.83}Co_{1.1}P_{0.6}Si_{0.4}$). The representations on the left illustrate the basic metal blocks, those on the right display the stacking of the blocks.

Table 2
Connection between the crystallographic sites (Wyckoff positions) in the three crystal structures.

BCO	Fe_2P-type	Co_2P-type
8*e*, 4*c*	metal 3*f* tetrahedron	4*c* (0.1443, ¼, 0.0607)
4*d*, 4*d*, 2*b*, 2*a*	metal 3*g* square-based pyramid	4*c* (0.0285, ¼, 0.6705)
8*e*	metalloid 2*c*	4*c*
2*a*, 2*b*	metalloid 1*b*	4*c*

two aspects. First, T_C no longer increases with Co for $y = 0.2$, as it barely shows any significant evolution, until decreasing in the orthorhombic range. For $y = 0.4$ and 0.5, T_C shows a reverse trend, it is actually decreasing with Co for Fe substitutions. The second puzzling result highlighted by the present $T_C(x,y)$ dataset is the apparent lack of a direct structure-property relationship within the stability range of the Fe_2P structure. The *c*/*a* ratio is systematically increasing with

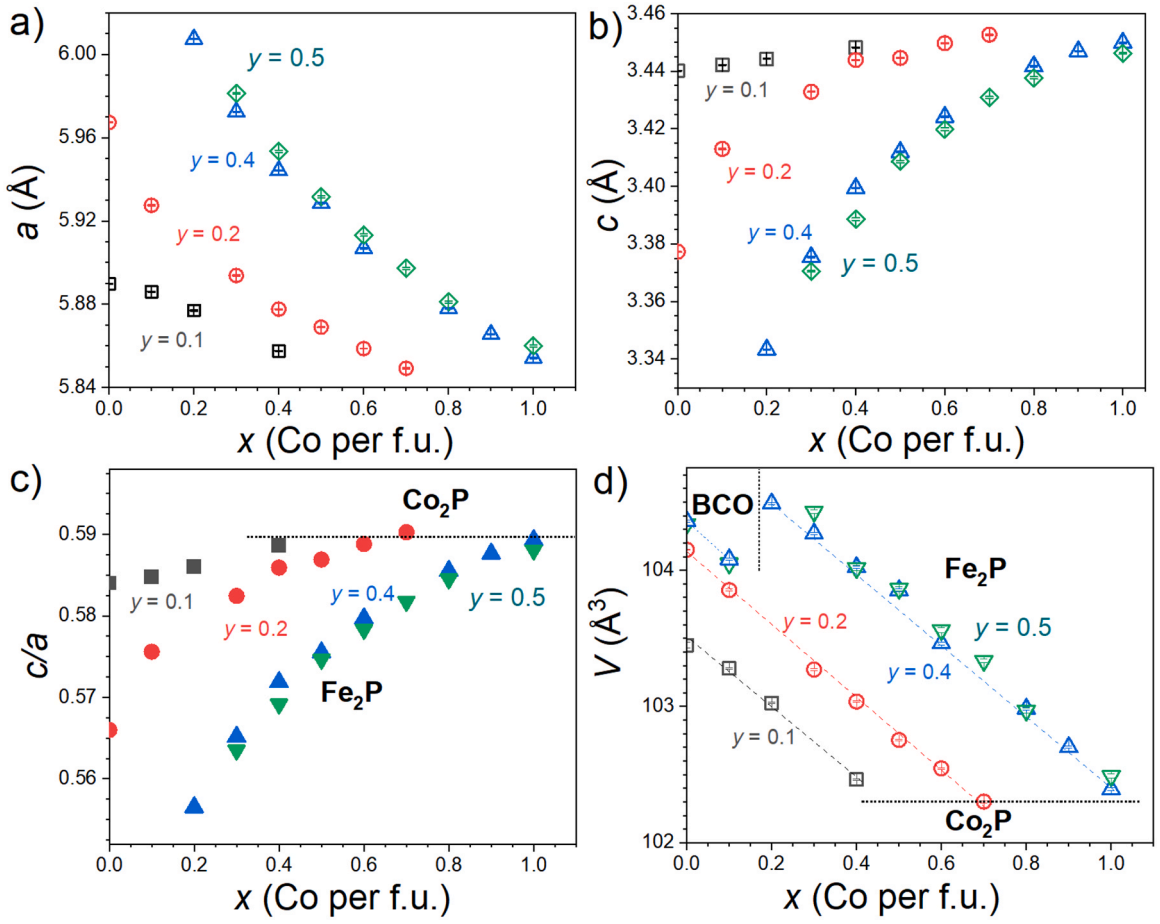

Fig. 5. Room-temperature lattice parameters *a* and *c* (panels a and b) and ratio *c/a* (panel c) for hexagonal Fe_2P-type $Fe_{1.93-x}Co_xP_{1-y}Si_y$ compounds, the unit-cell volume *V* (panel d) includes a few compositions crystallizing in the BCO structure.

Co substitutions in quaternary $Fe_{1.93-x}Co_xP_{1-y}Si_y$ compounds, while the Curie temperature can be increasing, unmodified or decreasing. This is at odds with the common belief that in Fe_2P materials magnetic properties are strongly influenced by structural modifications and in particular those affecting the *c/a* ratio. Generally, an increase in *c/a* is associated with a decrease in Curie temperature. This is in particular observed in magnetocaloric $(Mn,Fe)_2(P,Si)$ quaternary compounds. In Fe-rich $Mn_{0.66}Fe_{1.29}P_{1-y}Si_y$ compounds when Si increases, *c/a* decreases and T_C increases [25]. In Mn-rich compounds, $Mn_{1.25}Fe_{0.70}P_{1-y}Si_y$ when Si increases, *c/a* decreases and T_C increases [24]. In B-substituted $MnFe_{0.95}P_{2/3-y}Si_{1/3}B_y$, when B increases, the paramagnetic *c/a* decreases, the ferromagnetic *c/a* is not significantly affected and T_C increases [26]. In Co-substituted $MnFe_{0.95-x}Co_xP_{0.50}Si_{0.50}$ or $Mn_{1-x}Co_xFe_{0.95}P_{0.50}Si_{0.50}$, when the Co content increases, *c/a* increases and T_C decreases [27]. These experimental tendencies can be understood thanks to several theoretical studies on ternary or quaternary compounds derived from Fe_2P [17,28,29]. Most of them highlighted the important role played by the distance between the metallic 3*g* and 3*f* planes stacked along the *c* axis. In particular, a decrease in *c/a* ratio, i.e. a shrinkage of the distance between 3*f* and 3*g* sites, is expected to strengthen the magnetic 3*f*-3*g* interaction, favoring the development of a higher moment state on the 3*f* site and possibly an increase in Curie temperature. Clearly, in the present $Fe_{1.93-x}Co_xP_{1-y}Si_y$ quaternary compounds the evolution of the Curie temperature cannot be reduced to the effect of a single variable like the *c/a* ratio. Band filling and different magnetic moments due to Co substitutions may play a role. In addition, preferential site occupation cannot be resolved on the basis of the present XRD data. In *MM'X* materials, the usual trends are that the metal with the lowest *d* electrons will go in the pyramidal site

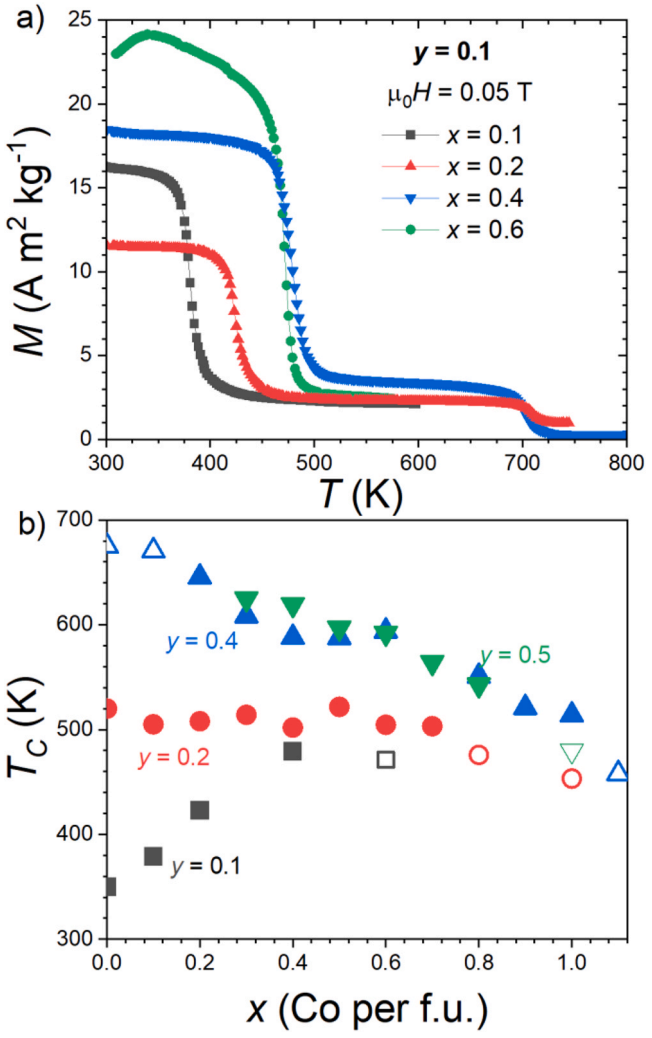

Fig. 6. Magnetic properties of $Fe_{1.93-x}Co_xP_{1-y}Si_y$ compounds. a) Temperature dependence of the magnetization for the $y = 0.1$ series. b) Curie temperatures (closed symbols for samples crystallizing in the Fe_2P-type structure, open symbols for BCO or Co_2P-type structures).

(3*g* for Fe_2P-type structure) and the largest metalloid will sit preferentially in the largest metalloid site (the 2*c* site for Fe_2P structure) [30].

This trend is confirmed in magnetocaloric $(Mn,Fe)_2(P,As)$ and $(Mn,Fe)_2(P,Si)$ compounds where a strong selectivity of Mn for the 3*g* site is observed [31,32] and a preferential occupation of Si on the 2*c* site [33]. We therefore expect that in $Fe_{1.93-x}Co_xP_{1-y}Si_y$ quaternaries, Co will preferentially substitute the 3*f* site and Si the 2*c* site in the Fe_2P structure. Yet, the degree of selectivity might be influenced by both the Co content and the level of Si substitution, which could play a role in the complex evolution of T_C with Co substitution.

The evolution of the magneto-crystalline anisotropy is crucial for future works on potential permanent magnet applications of $Fe_{1.93-x}Co_xP_{1-y}Si_y$ quaternary compounds. A preliminary study on $Fe_{1.8}Co_{0.2}P_{1-y}Si_y$ oriented powders with *x* fixed at 0.2 indicated that the *c* axis corresponds to the easy magnetic axis and that the magneto-crystalline anisotropy at room temperature tends to form an optimum for specific compositions ($y \sim 0.2$ for $x = 0.2$) [18]. These observations were recently confirmed by magnetization measurements on single-crystal samples [20,21]. However, the compositional range explored by these studies were limited. Fig. 7 presents diffraction patterns of representative $Fe_{1.93-x}Co_xP_{1-y}Si_y$ oriented and bounded powders and their magnetization curves. In line with previous studies [18,20], no significant magnetic hysteresis was observed at room temperature in the present bulk or coarse powder samples. A microstructural control, such as forming submicron-sized particles, would be required to induce permanent magnetic properties [20]. At low Si content, the XRD patterns of the oriented powders show a clear preferential orientation along the *c* axis. The sizable difference between $M(H)$ curves recorded with the measurement field applied parallel and perpendicular to the orientation field reveals a substantial magneto-crystalline anisotropy, but increasing the Co content appears to weaken it. When considering larger Si contents, e.g. $y = 0.4$ showing higher T_C, the magneto-crystalline anisotropy appears significantly weaker. These two observations are qualitatively in line with former polycrystalline and single-crystal studies [18–21]. We note that the oriented powder method may underestimate the actual magnetic anisotropy, as samples with a weak anisotropy at room temperature will more likely suffer from misorientations, and therefore would show an even more reduced anisotropy, which is potentially the case for the $x = 0.2$, $y = 0.4$ sample. For $y = 0.4$, at low Co content the easy magnetization direction remains the crystallographic *c* axis. But the oriented powder diffractogram of samples with larger Co substitutions ($x = 0.4$) are drastically different with an increased intensity of the reflections having an *a*-*b* basal plane component, indicating a change in the magneto-crystalline anisotropy scheme with moments tilted or oriented toward the *a*-*b* plane. Such a change in magnetic anisotropy is undesired for permanent magnet applications, in particular as it leads to a further reduction in magneto-crystalline anisotropy energy as indicated by the particularly small area between $M(H)$ curves recorded with the measurement field parallel and perpendicular to the orientation field. The present investigation shows that even if the Fe_2P structure can be maintained up to large Si ($y_{max} \approx 0.5$) and Co contents ($x_{max} \approx 1.0$), the preferred composition range for potential permanent magnetic properties corresponds to rather limited Co and Si substitutions, typically $x \lesssim 0.3$ and $y \lesssim 0.3$.

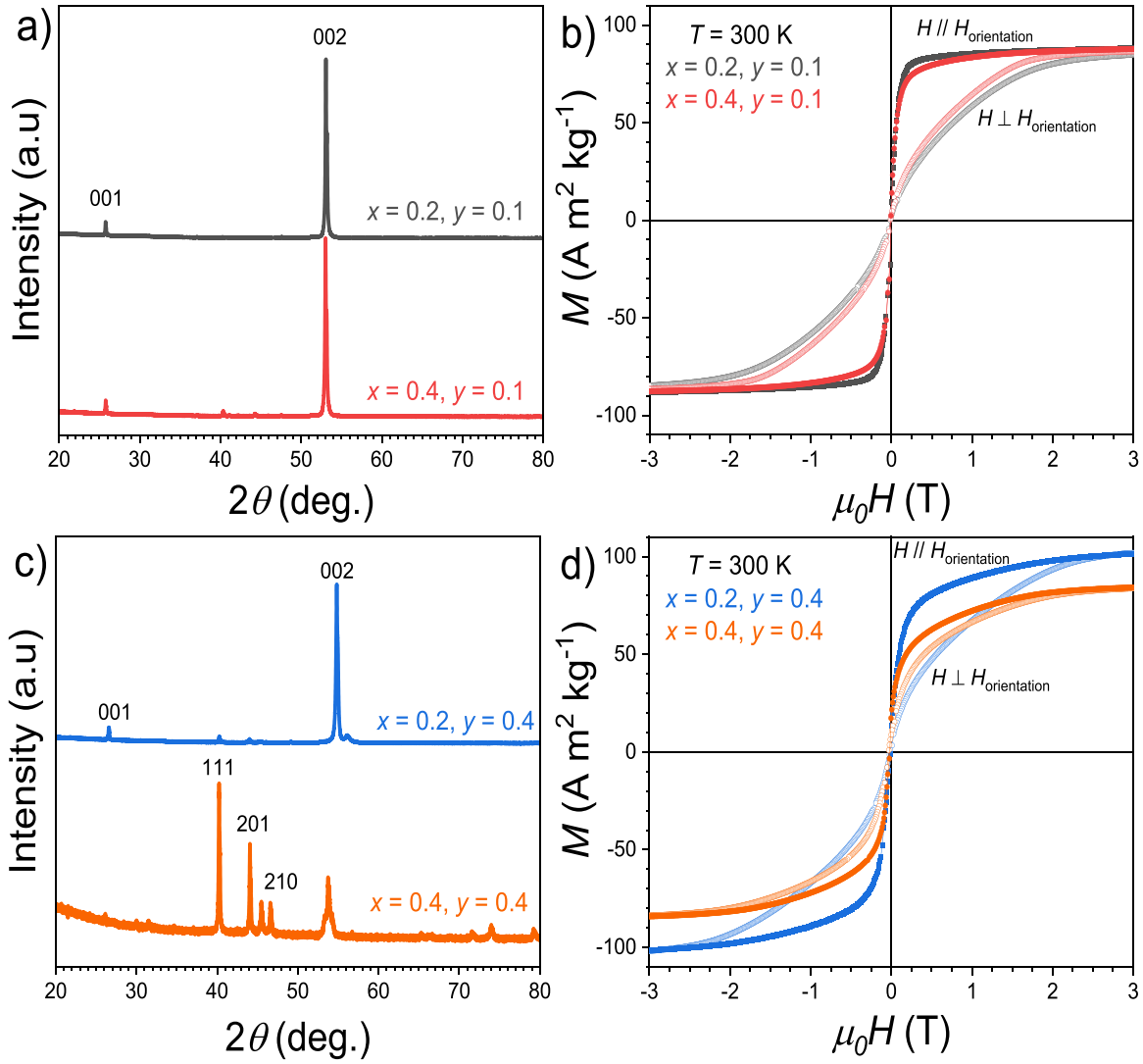

Fig. 7. XRD diffraction patterns and magnetization curves for oriented and bounded $Fe_{1.93-x}Co_xP_{1-y}Si_y$ powders.

4. Conclusions

The crystal and magnetic phase diagrams of quaternary $Fe_{1.93-x}Co_xP_{1-y}Si_y$ compounds were explored focusing on establishing the Fe_2P-type compositional range. Si for P substitutions compensate the cell volume reduction due to Co for Fe substitutions, delaying the appearance of the competing orthorhombic Co_2P-type structure to high Co contents ($x_{max} \approx 1.0$). Si for P substitutions decrease the *c/a* ratio of the lattice parameters and lead to an increase in Curie temperature. Co for Fe substitutions increase the *c/a* ratio, lead to an increase in T_C at low Si content, no sizable evolution for $y = 0.2$ and even a decrease in the Curie temperature for $y = 0.4$ and 0.5. This apparent lack of structure-magnetic ordering relationship with Co substitutions is unusual in materials derived from Fe_2P and calls for a dedicated study, in particular resolving possible preferential substitutions schemes for Si and Co. Magnetization curves recorded on oriented powder show that high Si and Co substitutions lead to a swift weakening of the magneto-crystalline anisotropy until the *c* easy axis anisotropy turns toward the *a-b* plane. This study guides further developments by demonstrating that the compositional range most desirable for permanent magnetic applications corresponds to $0.1 \lesssim x \lesssim 0.3$ and $0.1 \lesssim y \lesssim 0.3$.

CRediT authorship contribution statement

L.L. Bao: Investigations, Data curation, Writing – original draft. **H. Yibole:** Project administration, Supervision. **J.Y. Xu:** Investigations. **Z.Q. Ou:** Resources. **O. Haschuluu:** Resources. **O. Tegus:** Writing – review & editing. **N.H. van Dijk:** Writing – review & editing. **E. Brück:** Writing – review & editing. **F. Guillou:** Conceptualization, Writing – review & editing.

Declaration of Competing Interest

The authors declare that they have no known competing financial interests or personal relationships that could have appeared to influence the work reported in this paper.

Acknowledgements

The work is supported by the National Natural Science Foundation of China (grant numbers 11904188, 51961033, 11864031 and 52150610486), the Inner Mongolia Autonomous Region (grant numbers NJZY20025 and NJYT-20-A17) and the Inner Mongolia

Normal University (grant numbers CXJJS20098, 2018YJRC002 and 2018YJRC003).

References

[1] O. Gutfleisch, M.A. Willard, E. Brück, C.H. Chen, S.G. Sankar, J.P. Liu, Magnetic materials and devices for the 21st century: stronger, lighter, and more energy efficient, Adv. Mater. 23 (2011) 821–842, https://doi.org/10.1002/adma.201002180

[2] J.M.D. Coey, Permanent magnets: plugging the gap, Scr. Mater. 67 (2012) 524–529, https://doi.org/10.1016/j.scriptamat.2012.04.036

[3] J. Cui, M. Kramer, L. Zhou, F. Liu, A. Gabay, G. Hadjipanayis, B. Balasubramanian, D. Sellmyer, Current progress and future challenges in rare-earth-free permanent magnets, Acta Mater. 158 (2018) 118–137, https://doi.org/10.1016/j.actamat.2018.07.049

[4] J. Mohapatra, J.P. Liu, Chapter 1 - rare-earth-free permanent magnets: the past and future, Handb. Magn. Mater. 27 (2018) 1–57, https://doi.org/10.1016/bs.hmm.2018.08.001

[5] R. Wäppling, L. Häggström, T. Ericsson, S. Devanarayanan, E. Karlsson, B. Carlsson, S. Rundqvist, First order magnetic transition, magnetic structure, and vacancy distribution in Fe_2P, J. Solid. State Chem. 13 (1975) 258–271, https://doi.org/10.1016/0022-4596(75)90128-0

[6] H. Fujii, T. Hokabe, T. Kamigaichi, T. Okamoto, Magnetic properties of Fe_2P single crystal, J. Phys. Soc. Jpn. 43 (1977) 41–46, https://doi.org/10.1143/JPSJ.43.41

[7] L. Lundgren, G. Tarmohamed, O. Beckman, B. Carlsson, S. Rundqvist, First order magnetic phase transition in Fe_2P, Phys. Scr. 17 (1978) 39–48, https://doi.org/10.1016/0022-4596(75)90128-0

[8] L. Caron, M. Hudl, V. Höglin, N.H. Dung, C.P. Gomez, M. Sahlberg, E. Brück, Y. Andersson, P. Nordblad, Magnetocrystalline anisotropy and the magnetocaloric effect in Fe_2P, Phys. Rev. B 88 (2013) 094440, https://doi.org/10.1103/PhysRevB.88.094440

[9] R. Fruchart, A. Roger, J.P. Senateur, Crystallographic and magnetic properties of solid solutions of the phosphides M_2P, M = Cr, Mn, Fe, Co, and Ni, J. Appl. Phys. 40 (1969) 1250–1257, https://doi.org/10.1063/1.1657617

[10] H. Fujii, T. Hokabe, T. Kamigaichi, H. Fujiwara, T. Okamoto, Magnetic properties of single crystals of the system $(Fe_{1-x}Ni_x)_2P$, J. Phys. Soc. Jpn. 44 (1978) 96–100, https://doi.org/10.1143/JPSJ.44.96

[11] R. Chandra, S. Bjarman, T. Ericsson, L. Häggström, C. Wilkinson, R.A. Wäppling, Mössbauer and X-ray study of $Fe_2P_{1-x}B_x$ compounds ($x < 0.15$), J. Solid State Chem. 34 (1980) 389–396, https://doi.org/10.1016/0022-4596(80)90440-5

[12] P. Jernberg, A.A. Yousif, L. Häggström, Y. Andersson, A. Mössbauer, study of $Fe_2P_{1-x}Si_x$ ($x \leq 0.35$), J. Solid State Chem. 53 (1984) 313–322, https://doi.org/10.1016/0022-4596(84)90108-7

[13] A. Catalano, R.J. Arnott, A. Wold, Magnetic and crystallographic properties of the system $Fe_2P_{1-x}As_x$, J. Solid State Chem. 7 (1973) 262–268, https://doi.org/10.1016/0022-4596(73)90132-1

[14] K.J. de Vos, W.A.J.J. Velge, M.G. van der Steeg, H. Zijlstra, Permanent magnetic properties of iron-cobalt-phosphides, J. Appl. Phys. 33 (1962) 1320–1322, https://doi.org/10.1063/1.1728712

[15] Y. Tokuoka, J. Yoshinari, Ferromagnetic stabilized ultrafine spherical hexagonal crystalline Fe2P particles. United States Patent US 005277977, 1994.

[16] D. Li, M.P. Arachchige, B. Kulikowski, G. Lawes, T. Seda, S.L. Brock, Control of composition and size in discrete $Co_xFe_{2-x}P$ nanoparticles: consequences for magnetic properties, Chem. Mater. 28 (2016) 3920–3927, https://doi.org/10.1021/acs.chemmater.6b01185

[17] I.A. Zhuravlev, V.P. Antropov, A. Vishina, M. van Schilfgaarde, K.D. Belashchenko, Tunable dimensional crossover and magnetocrystalline anisotropy in Fe_2P-based alloys, Phys. Rev. Mater. 1 (2017) 051401(R), https://doi.org/10.1103/PhysRevMaterials.1.051401

[18] F. Guillou, Sun Liting, O. Haschuluu, Z.Q. Ou, E. Brück, O. Tegus, H. Yibole, Room temperature magnetic anisotropy in Fe_2P-type transition metal based alloys, J. Alloy. Compd. 800 (2019) 403–411, https://doi.org/10.1016/j.jallcom.2019.05.327

[19] J.Y. Xu, Lingling Bao, H. Yibole, F. Guillou, Structure and magnetic properties of $Fe_{1.95-x}Ni_xP_{1-y}Si_y$ alloys, Solid State Commun. 319 (2020) 113996, https://doi.org/10.1016/j.ssc.2020.113996

[20] H. Yibole, Lingling Bao, J.Y. Xu, H. Alata, O. Tegus, W. Hanggai, N.H. van Dijk, E. Brück, F. Guillou, $(Fe,Co)_2(P,Si)$ rare-earth free permanent magnets: from macroscopic single crystals to submicron-sized particles, Acta Mater. 221 (2021) 117388, https://doi.org/10.1016/j.actamat.2021.117388

[21] Y. He, P. Adler, S. Schneider, I. Soldatov, Q. Mu, H. Borrmann, W. Schnelle, R. Schaefer, B. Rellinghaus, G.H. Fecher, C. Felser, Intrinsic magnetic properties of a highly anisotropic rare-earth-free Fe_2P-based magnet, Adv. Funct. Mater. (2021), https://doi.org/10.1002/adfm.202107513

[22] J. Rodríguez-Carvajal, Recent advances in magnetic structure determination by neutron powder diffraction, Phys. B: Condens. Matter 192 (1993) 55–69, https://doi.org/10.1016/0921-4526(93)90108-I

[23] K. Momma, F. Izumi, VESTA 3 for three-dimensional visualization of crystal, volumetric and morphology data, J. Appl. Crystallogr. 44 (2011) 1272–1276, https://doi.org/10.1107/S0021889811038970

[24] H.D. Nguyen, Moment Formation and Giant Magnetocaloric Effects in Hexagonal Mn-Fe-P-Si Compounds, Ph.D. Thesis, TU Delft, 2012, https://doi.org/10.4233/uuid:11afb8c7-ddd4-42a9-baa1-33cebe05b3b0

[25] Z.Q. Ou, Magnetic Structure and Phase Formation of Magnetocaloric Mn-Fe-P-X Compounds Ph.D. Thesis, TU Delft, 2013, https://doi.org/10.4233/uuid:4ba9f9cb-49fe-48a2-ab89-eb80070b7362

[26] F. Guillou, H. Yibole, N.H. van Dijk, E. Brück, Effect of boron substitution on the ferromagnetic transition of $MnFe_{0.95}P_{2/3}Si_{1/3}$, J. Alloy. Compd. 632 (2015) 717–722, https://doi.org/10.1016/j.jallcom.2015.01.308

[27] Z.Q. Ou, N.H. Dung, L. Zhang, L. Caron, E. Torun, N.H. van Dijk, O. Tegus, E. Brück, Transition metal substitution in Fe_2P-based $MnFe_{0.95}P_{0.50}Si_{0.50}$ magnetocaloric compounds, J. Alloy. Compd. 730 (2018) 392–398, https://doi.org/10.1016/j.jallcom.2017.09.315

[28] E.K. Delczeg-Czirjak, Z. Gercsi, L. Bergqvist, O. Eriksson, L. Szunyogh, P. Nordblad, B. Johansson, L. Vitos, Magnetic exchange interactions in B-, Si-, and As-doped Fe_2P from first-principles theory, Phys. Rev. B 85 (2012) 224435, https://doi.org/10.1103/PhysRevB.85.224435

[29] Z. Gercsi, E.K. Delczeg-Czirjak, L. Vitos, A.S. Wills, A. Daoud-Aladine, K.G. Sandeman, Magnetoelastic effects in doped Fe_2P, Phys. Rev. B 88 (2013) 024417, https://doi.org/10.1103/PhysRevB.88.024417

[30] A. Nylund, A. Roger, J.P. Sénateur, R. Fruchart, Evolution structurale des phosphures, arséniures et arséniophosphures M_2P, M_2As et $M_2(P_{1-x}As_x)$, J. Solid State Chem. 4 (1972) 115–122, https://doi.org/10.1016/0022-4596(72)90139-9

[31] M. Bacmann, J.L. Soubeyroux, R. Barrett, D. Fruchart, R. Zach, S. Niziol, R. Fruchart, Magnetoelastic transition and antiferro-ferromagnetic ordering in the system $MnFeP_{1-y}As_y$, J. Magn. Magn. Mater. 134 (1994) 59–67, https://doi.org/10.1016/0304-8853(94)90073-6

[32] N.H. Dung, L. Zhang, Z.Q. Ou, L. Zhao, L. van Eijck, A.M. Mulders, M. Avdeev, E. Suard, N.H. van Dijk, E. Brück, High/low-moment phase transition in hexagonal Mn-Fe-P-Si compounds, Phys. Rev. B 86 (2012) 045134, https://doi.org/10.1103/PhysRevB.86.045134

[33] X.F. Miao, L. Caron, P. Roy, N.H. Dung, L. Zhang, W.A. Kockelmann, R.A. de Groot, N.H. van Dijk, E. Brück, Tuning the phase transition in transition-metal-based magnetocaloric compounds, Phys. Rev. B 89 (2014) 174429, https://doi.org/10.1103/PhysRevB.89.174429